Quasi-retroreflection from corner cubes with refractive free-form surfaces

Shin-Woong Park,[1] Eunkyong Moon,[2] Hayun Chung,[2] Joon-Yong Lee,[3] Chanyeol Bae,[3] Jin-Woo Kim,[3] and Hwi Kim[2,*]

[1]Center for Advanced Photovoltaic Materials, Korea University, 2511 Sejong-ro, Sejong 339-700, South Korea

[2]ICT Convergence Technology for Health & Safety and Department of Electronics and Information Engineering, Korea University, 2511 Sejong-ro, Sejong 339-700, South Korea

[3]MNtech Co., Ltd. 16 Gwahaksaneop 1-ro, Oksan-myeon, Cheongwon-gun, Chungcheongbuk-do 363-911, South Korea

*Corresponding author: hwikim@korea.ac.kr

Received 3 July 2014; revised 15 August 2014; accepted 27 August 2014; posted 28 August 2014 (Doc. ID 216320); published 1 October 2014

Quasi-retroreflection from corner-cube structures with a refractive free-form surface is studied. It is shown that adjustment of the structural parameters of the free-form surface allows control of quasi-retroreflection. Quasi-retroreflection corner-cube array sheets with specified quasi-retroreflection angle are modeled, and their quasi-retroreflection characteristics are analyzed.

OCIS codes: (080.2740) Geometric optical design; (120.5700) Reflection; (120.4570) Optical design of instruments.

http://dx.doi.org/10.1364/AO.53.006605

1. Introduction

Retroreflection is a well-known optical phenomenon [1,2] that has been applied to a wide range of applications such as traffic signage [3], 3D displays [4–6], head-mounted displays [7,8], adaptive optics [9], and noncontact range sensors [10,11]. In practice, corner-cube structure is popularly used to generate retroreflection [12]. Theoretically, perfect retroreflection occurs by a corner cube with 90° dihedral angles. However, in many practical applications, imperfect retroreflection with a finite divergence, i.e., quasi-retroreflection, is more desirable than perfect retroreflection [13,14]. For example, for traffic signage and safety applications, quasi-retroreflection rather than perfect retroreflection is necessary because the headlight of an automobile directed toward traffic signage should be reflected toward the driver's head rather than the headlight lamp, i.e., light source, as shown in Fig. 1. The observation direction represented by observation angle β is not parallel to the light illumination direction parameterized by the entrance (incidence) angle α.

The quasi-retroreflection function that is required for the traffic signage cannot be achieved, if it has perfect corner-cube arrays. According to the ASTM standard [3], the performance of the traffic signage application is evaluated by measuring the quasi-retroreflection efficiencies for the entrance angles of −4° and 30° at the observation angles of −0.5° and 1°. Therefore, quasi-retroreflection control along the vertical direction is required for traffic signage applications, as can be seen in Fig. 1.

In general, such quasi-retroreflection characteristics are realized through statistical variation in fabrication control or artificial deviations from perfection in corner-cube fabrication. In our previous study [14], quasi-retroreflection induced by a positional error at the apex point of the corner-cube structure was analyzed. In this case, however, quasi-retroreflection is not controllable, but merely

1559-128X/14/286605-07$15.00/0

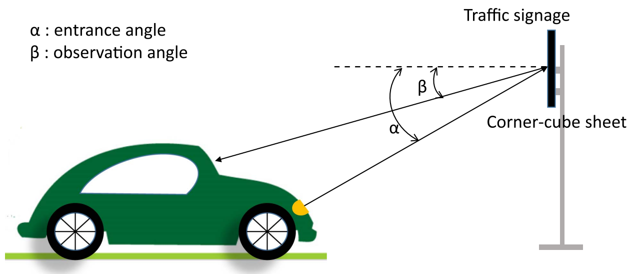

Fig. 1. Automobile traffic application of quasi-retroreflection: entrance and observation angles are denoted by α and β, respectively.

randomized imperfect retroreflection. In [14], even a small positional deviation of the apex point of the corner cube induces a considerable divergent quasi-retroreflection spectrum profile on the directional vector space. The generation of controlled quasi-retroreflection using the adjustment of the apex point position is difficult and not robust.

In this paper, we propose a corner-cube structure with a trapezoid free-form surface structure designed for generating precisely controlled quasi-retroreflection that can be broadened either vertically or horizontally. It is shown that the divergence angle of the quasi-retroreflection and retroreflection efficiency can vary with adjustment of the structural parameters. As a result, the objective design of the optimal quasi-retroreflection corner-cube structure with the quasi-retroreflection angle of 1° is presented with geometrical optic simulation of the quasi-retroreflection patterns of the designed corner-cube sheets.

This paper is organized as follows. In Section 2, a geometric model of the quasi-retroreflection corner-cube structure and the design principle are described. In Section 3, parametric study of variations in the quasi-retroreflection pattern and efficiency is conducted. In Section 4, based on the analytical results, the optimal design of the quasi-retroreflection corner-cube sheet is modeled, and its quasi-retroreflection property is characterized. Finally, a conclusion is given in Section 5.

2. Geometric Model of Quasi-Retroreflection Corner Cube

Before addressing our main idea about quasi-retroreflection, we review briefly the basic properties of the perfect retroreflection by a triangular pyramid corner cube in Fig. 2(a). A ray with directional vector $\mathbf{k}_{\mathrm{inc}} = (k_x, k_y, k_z)$ is incident on the entrance facet $P_1P_2P_3$. The incident ray is reflected three times at the orthogonal inclined facets of the corner cube and exits from the entrance facet with directional vector, $\mathbf{k}_{\mathrm{ref}} = -(k_x, k_y, k_z)$. Because the ray makes a round trip inside the corner-cube structure, the exit position is slightly shifted from the entrance position by $\Delta\mathbf{r}$, as shown in Fig. 2(a), but the reflected ray is still parallel to the incident ray. In this case, the retroreflection pattern can be taken by a superposition of many effective retroreflection areas that are shifted transversally, in the detector plane distant from the retroreflection corner cube [12,15,16].

In general, positional shift $\Delta\mathbf{r}$ may be dependent on various structural parameters such as incidence angle, incidence position, and dimensions of the corner cube. In Fig. 2(b), we illustrate a design of the corner-cube structure with a shallow and transparent 1D periodic trapezoid refractive free-form surface for generating quasi-retroreflection.

The mechanism of quasi-retroreflection generation in the proposed structure can be understood in terms of the combination of the entrance–exit facet pair of the corner-cube structure. Consider the ray that is incident on a facet, transmitted onto the effective retroreflection area of the corner cube, and continues to travel inside the corner cube and returns to the free-form structure. As mentioned above, the entrance and exit points are separated by a spatial shift, $\Delta\mathbf{r}$. The entrance and exit points of a ray can exist on the same facet of the free-form surface, even with shift $\Delta\mathbf{r}$, or assigned on separate unparalleled facets. In the former case, the ray is perfectly retroreflected, but quasi-retroreflection of the ray with a

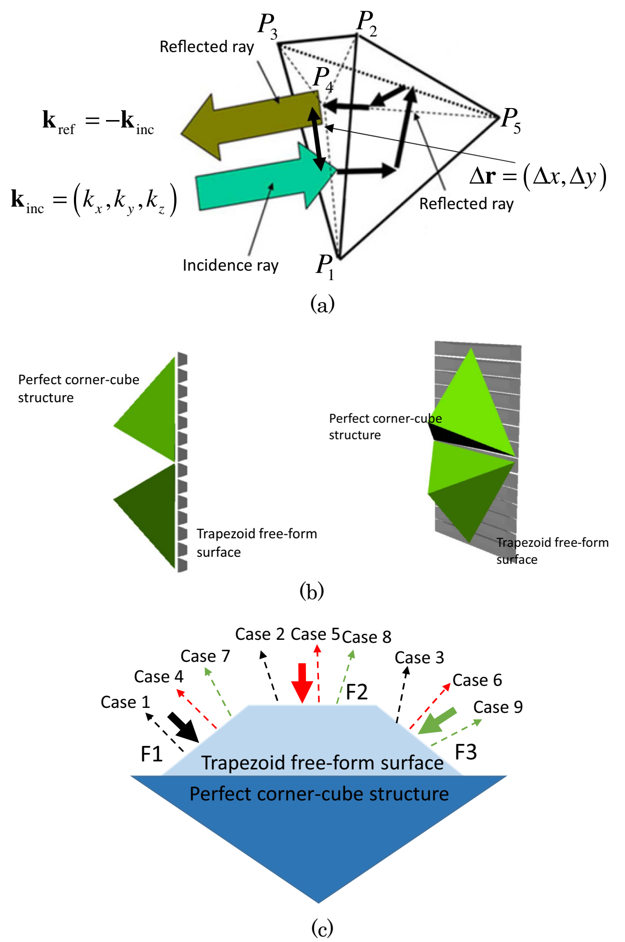

Fig. 2. (a) Perfect retroreflection in a corner-cube structure. (b) Proposed quasi-retroreflection corner-cube structure with trapezoid free-form surface. (c) Generation of perfect and quasi-retroreflections according to the combination of entrance–exit pair at the trapezoid free-form surface.

Table 1. Classification of Retroreflection with respect to Combination of Incidence Entrance and Reflection Exit Facets

Case	Entrance	Exit	Retroreflection
1	F1	F1	Perfect
2	F1	F2	Quasi
3	F1	F3	Quasi
4	F2	F1	Quasi
5	F2	F2	Perfect
6	F2	F3	Quasi
7	F3	F1	Quasi
8	F3	F2	Quasi
9	F3	F3	Perfect

considerable deviation from the perfect retroreflection path is induced for the latter case. We can classify retroreflection types according to the permutative combination of entrance–exit facet pairs. Regarding the proposed structure depicted in Fig. 2(b), we identify three possible cases of entrance–exit combinations (F1–F1, F2–F2, and F3–F3) for perfect retroreflection and a total of six cases for quasi-retroreflection, which are listed in Table 1. If both entrance and exit facets of a ray are the same (for example, F1), the reflected ray is parallel to the incident ray, which corresponds to the perfect retroreflection case. On the other hand, if the exit facet is facet F2, the refracted ray to free space is not parallel to the incident ray. Also, the degree of deviation is dependent on the directional difference between the surface normal vectors of the entrance and exit facets. The surface normal vectors can be controlled by adjusting the base angles and height of the trapezoid unit.

3. Control of Quasi-Retroreflection by Structural Parameters

The proposed quasi-retroreflection structure is modeled and analyzed by ZEMAX software. In Fig. 3, the simulation setup is schematically shown. Rays emitted from a point source are illuminated on the entrance facet of the pair of two triangular pyramid corner cubes with free-form surface array. Here, the unit of the free-form surface array is assumed to be a trapezoidal form parameterized by base angle φ and flat plane width m. Width m corresponds to the flat facet F2 in Fig. 2(c). The reflected rays are measured by a flat rectangular power detector distant from the structure. The detector used in ZEMAX

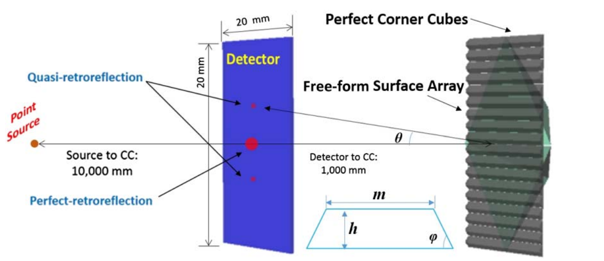

Fig. 3. ZEMAX modeling of the proposed quasi-retroreflection corner cube.

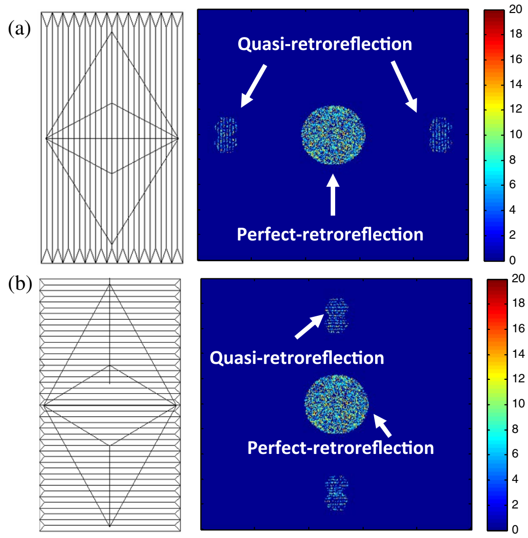

Fig. 4. (a) ZEMAX modeling and simulation results of the quasi-retroreflection corner-cube structures with (a) vertical and (b) horizontal prism arrays on their entrance facets.

modeling is transparent to the source, but records the rays emitted from the corner-cube pair. The focus of the analysis is the control of reflection angle and power of quasi-retroreflection.

In Figs. 4(a) and 4(b), prism arrays are attached on the entrance facet in the vertical and horizontal directions, respectively. The refractive indices of the prism and corner cube, period of the prism array, and edge size of the regular triangular corner cube are set to 1.5, 0.2, and 2.4 mm, respectively. According to Cases 3 and 7 in Table 1, two quasi-retroreflection beams are generated by those configurations. The pattern captured by the detector verifies the generation of quasi-retroreflection. Interestingly, the quasi-retroreflection patterns reflect the effective retroreflection area of the corner-cube pair.

We conduct the parametric study on quasi-retroreflection variation with prism base angle φ and the topside flat plane width of trapezoid m of the proposed structure. In Figs. 5 and 6, the quasi-retroreflection patterns that vary with the base angle are presented. A considerable change in the reflection angle with the base angle of the prism sheet is clearly observed, confirming that the quasi-retroreflection angles are controlled by the base angle.

The relationship between the observation angle and the base angle is plotted in Fig. 7(a). Analysis shows that observation angle β is proportional to base angle ϕ without respect to whether the prism array is placed in the horizontal or vertical direction.

The quasi-retroreflection associated with Case 3 is geometrically analyzed in Fig. 7(b). Let the base angle of the trapezoid grating, incidence angle of an illumination ray measured from the surface normal of the incidence facet, and the refraction angle measured from the surface normal of the refraction facet be denoted by φ, ϕ, and γ, respectively. At the incidence facet, the refraction angle of the illumination ray, ψ, is solved by n and ϕ:

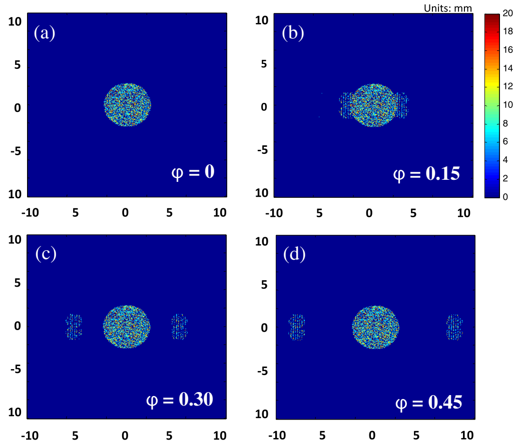

Fig. 5. Quasi-retroreflection patterns in horizontal gratings for various base angles, φ, (a) $\varphi = 0°$, (b) $\varphi = 0.15°$, (c) $\varphi = 0.30°$, and (d) $\varphi = 0.45°$. The relation of the observation angle to the base angle is represented graphically.

$$n \sin \psi = \sin \phi. \tag{1}$$

The refracted ray is retroreflected to meet the refracting facet. Refraction angle γ is obtained from Snell's law at the surface of the refraction facet as

$$n \sin(2\varphi - \psi) = \sin \gamma. \tag{2}$$

The angle deviation of the quasi-retroreflection from the perfect retroreflection is obtained by

$$\delta = \delta(\varphi, \phi; n) = \gamma + \phi - 2\varphi, \tag{3}$$

which is equal to the difference between the observation and entrance angles. The angle deviation of the quasi-retroreflection, $\delta = \delta(\varphi, \phi; n) = \gamma + \phi - 2\varphi$, is plotted with base angle φ and entrance angle, $\alpha = \phi - \varphi$. When entrance angle α is zero, i.e., normal incidence, observation angle β is equal to angle deviation, δ.

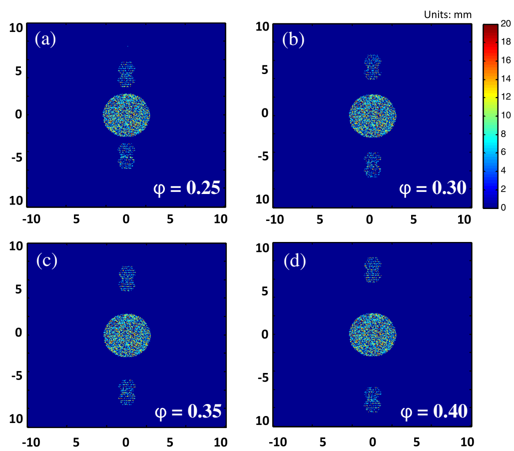

Fig. 6. Quasi-retroreflection patterns in vertical gratings for various base angles, φ, (a) $\varphi = 0.25°$, (b) $\varphi = 0.30°$, (c) $\varphi = 0.35°$, and (d) $\varphi = 0.40°$. The relation of the observation angle to the base angle is represented graphically.

The angle deviation graph of δ for the normal incidence angle in Fig. 7(c) accords well with the ZEMAX simulation result in Fig. 7(b). As entrance angle $\alpha = \phi - \varphi$ increases, the angular deviation of the quasi-retroreflection is also amplified. For example, for the entrance angle of 60° and the base angle of 1°, the angle deviation of the quasi-retroreflection reaches 2.8°. Figure 7(c) shows the effect of the entrance angle on the deviation of the quasi-retroreflection. For the other cases in Table 1, similar analytic formulas of the angular deviation of the quasi-retroreflection can be constructed.

On the other hand, the power ratio of quasi-retroreflection to the perfect retroreflection and the total power sum of those two cases transcend analytic description, and their analysis necessitates numerical analysis. The power of the quasi-retroreflection with varying topside flat plane width of the trapezoid structure is measured. In Fig. 8, the

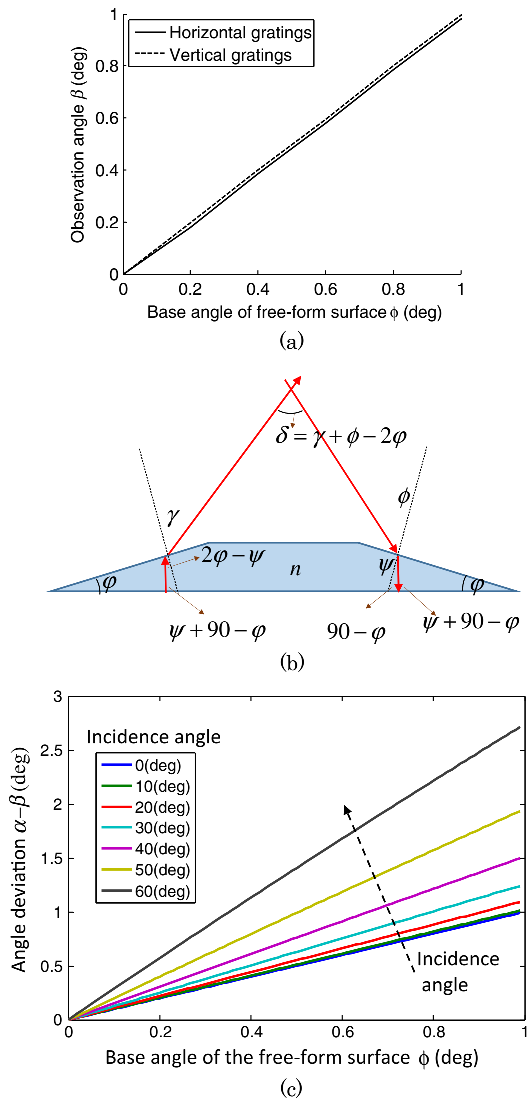

Fig. 7. (a) Observation angle distribution versus base angle of the free-form surface. (b) Geometry for analysis of Case 3. (c) Angle deviation of δ for the normal incidence angles.

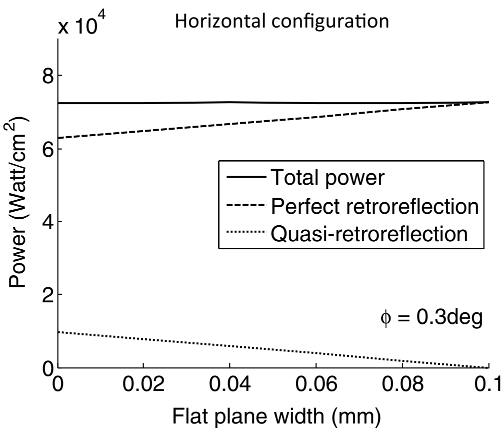

(a)

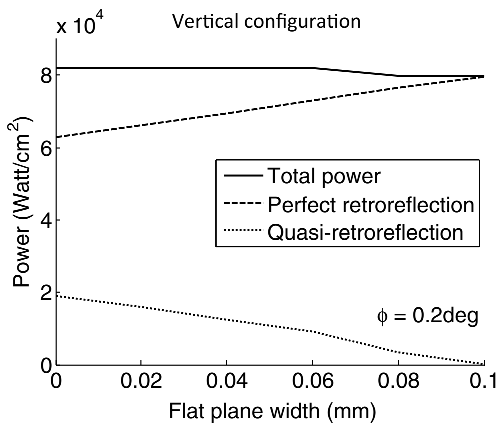

(b)

Fig. 8. Quasi-retroreflection power ratios for (a) horizontal configuration and (b) vertical configuration of the surface free-form structure.

quasi-retroreflection powers of the horizontal and vertical configurations of the free-form structures are tested with variation in m. As the topside flat plane width extends, the reflection efficiency of perfect retroreflection increases, but the quasi-retroreflection decreases, revealing a trade-off relation of the regular and quasi-retroreflections mediated by the topside flat plane width. For comparison, the total reflection power is plotted for flat plane width m in Fig. 8.

When parameter m is zero, the free-form surface forms a periodic prism array structure. In this case, the highest power of quasi-retroreflection is obtained. Varying parameter m, the total reflection power being equal to the sum of the perfect-retroreflection and quasi-retroreflection stays almost constant.

However, as the flat plane width m widens, the amount of the perfect retroreflection of Case 5 becomes significant, the quasi-retroreflection power decreases gradually with flat plane width m. The analysis shows that the topside flat plane width of the free-form surface is an effective control parameter of quasi-retroreflection, but the power ratio of the quasi-retroreflection is limited by an upper bound value of about 30%. On the prism structure with $m = 0$, the inclined facets, F1 and F2, constrained the increase of the quasi-retroreflection since the perfect retroreflections categorized by Cases 1 and 9 become dominant. Quasi-retroreflection is supported by Cases 3 and 7. At this point, the geometric ratio of the quasi-retroreflection reaches approximately 30%.

4. Quasi-Retroreflection Corner-Cube Sheets

Analysis is extended to a more practical array sheet form of the proposed quasi-retroreflection corner-cube structure [15–18]. In Fig. 9(a), the optical setup of characterizing the quasi-retroreflection property of the corner-cube sheet is schematically illustrated. A point-wise source with a cone-shaped divergent radiant profile shines sufficiently wide to cover the target corner-cube sheet away from the source by distance d. When collecting the far-field directional profile of the retroreflection of the target object with the hemispherical polar detector, i.e., the angular spectrum profile in the directional cosine vector space, we can employ the equivalent optical setup depicted in Fig. 9(b) for efficiency ZEMAX analysis. It represents the large area source emitting converging ray bundles being directed to the corner-cube unit and covering its entrance facet. The retroreflection pattern of a corner-cube unit fixed at the upper-right corner of the corner-cube sheet, shown in Fig. 9(a), which is recorded by the polar detector, is approximated by that of the corner-cube unit illuminated

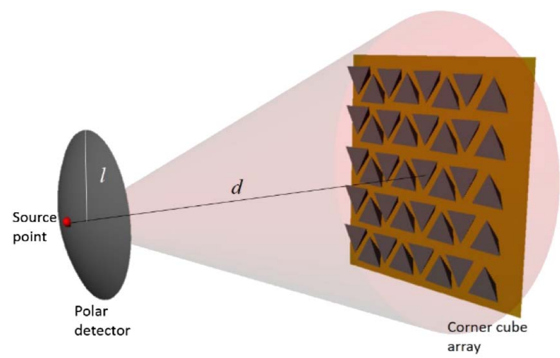

(a)

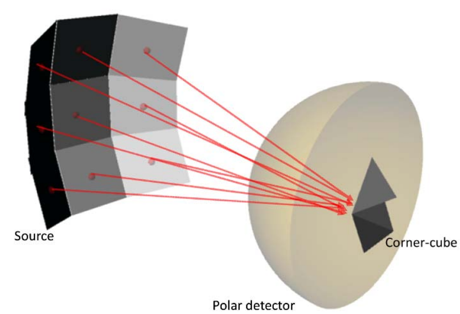

(b)

Fig. 9. (a) Perfect retroreflection in a corner-cube structure. (b) Quasi-retroreflection by a corner-cube structure with a triangular surface relief.

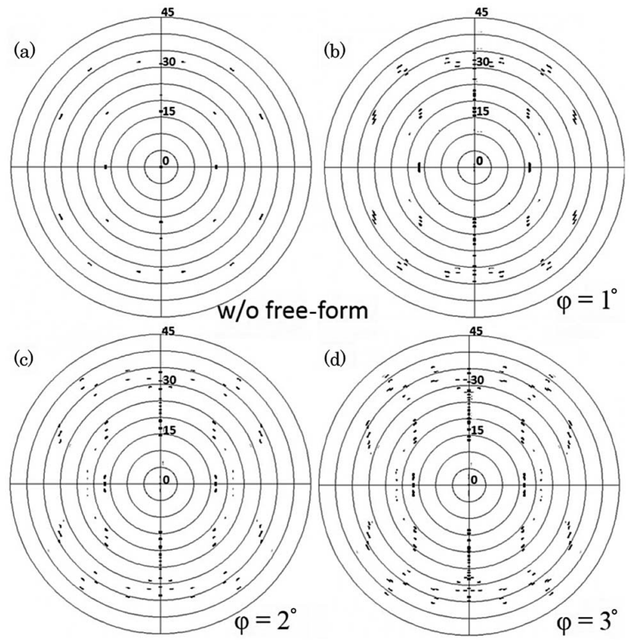

Fig. 10. Reflection patterns represented in the polar detector for (a) perfect retroreflection with base angle of $\varphi = 0°$ and quasi-retroreflection with base angles of (b) $\varphi = 1°$, (c) $\varphi = 2°$, and (d) $\varphi = 3°$. The source is distant by $d = 200$ mm from the corner-cube sheet.

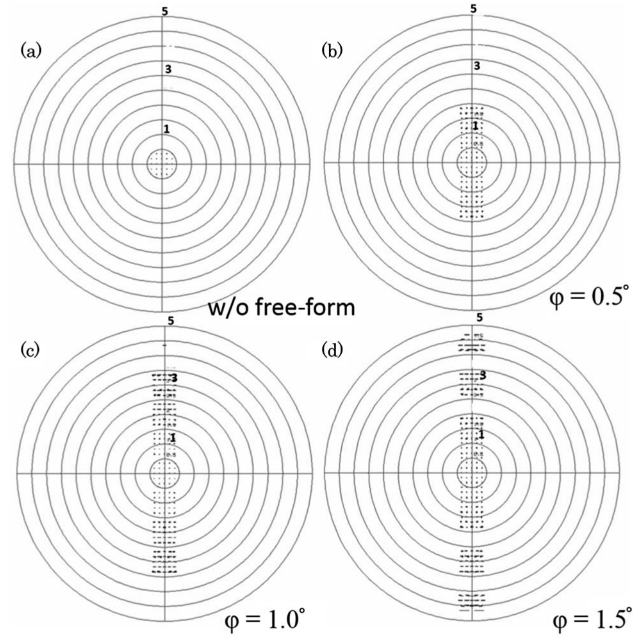

Fig. 11. Reflection patterns represented in the polar detector for (a) perfect retroreflection with base angle of $\varphi = 0°$ and quasi-retroreflection with base angles of (b) $\varphi = 0.5°$, (c) $\varphi = 1.0°$, and (d) $\varphi = 1.5°$. The source is distant by $d = 20000$ mm from the corner-cube sheet.

by the partial source localized around the lower-left corner of the extended source.

For the corner-cube sheet simulation, we employ the polar detector that resolves the angular spectrum profile in the directional cosine vector space. Figures 10 and 11 present the reflection light pattern measured by the polar detector for four free-form surfaces with a few base angles, where distance d of the source from the sample are, respectively, set to $d = 200$ mm and $d = 20000$ mm. The light source is taken by a 5×5 matrix configuration. For a source specified at a fixed distance of $d = 200$ mm and size of 240×240 mm, we vary the base angle as $\varphi = 0°$, $\varphi = 1°$, $\varphi = 2°$, and $\varphi = 3°$ and measure the reflection spectra at the polar detector. As proven in the previous analysis, the nonzero base angle induces quasi-retroreflection.

In the simulation, the free-form surface is horizontally arranged on the entrance surface of the corner cube. The free-form surface induces a split of the perfect retroreflection along the vertical direction. In practice, the light source is quite distant from the corner cube. The solid angle covered by the corner-cube sample narrows. The reflection spectrum of this case with $d = 20000$ mm is presented in Fig. 11. The angular bandwidth of the incident light source is set to be smaller than 0.5°. The perfect retroreflection of the corner-cube sheet is plotted in Fig. 11(a). The attachment of the free-form surface induces a broadening in the measured light pattern, which is ascribed to the generation of quasi-retroreflection in the entire area of the corner-cube sheet. Fine tuning of the base angle controls the vertical extension of the reflection light pattern on the hemispherical detector. We have shown that the deterministic controllability of quasi-retroreflection can be achieved by adjustment of the structural parameters of the free-form surface structure.

5. Conclusion

In conclusion, we have analyzed the quasi-retroreflection from a corner-cube structure with a trapezoid refractive free-form surface structure and shown that the adjustment of the surface free-form structure allows control of the quasi-retroreflection profile and its efficiency. The optimal quasi-retroreflection corner-cube sheet for specified observation angle can be designed based on the proposed method. In practice, the proposed structure is feasible for manipulating high-performance retroreflection sheets.

This research was supported by a grant from the World-Class 300 Project R&D Program and the Industrial Strategic Technology Development Program (no. 10042797, development of master machining system and 10% energy saving molding system for 100 nm–100 μm hybrid structures) funded by the Ministry of Knowledge Economy, Republic of Korea.

References

1. "Retroreflection: Definition and Measurement," CIE54.202001 (Commission International de L'Eclairage, 2001).
2. R. B. Nilsen and X. J. Lu, "Retroreflection technology," Proc. SPIE **5616**, 47–60 (2004).

3. “Standard specification for retroreflective sheeting for traffic control” ASTM Standard D4956-13 (ASTM International, 2013).
4. G. J. Woodgate, D. Ezra, J. Harrold, N. S. Holliman, G. R. Jones, and R. R. Moseley, “Observer tracking autostereoscopic 3D display systems,” Proc. SPIE **3012**, 187–198 (1997).
5. P. Harman, “Retroreflective screens and their application to autostereoscopic displays,” Proc. SPIE **3012**, 145–153 (1997).
6. B. Song, S. Choi, H. Sung, and S.-W. Min, “Reflection-type three-dimensional screen using retroreflector,” J. Opt. Soc. Korea **18**, 225–229 (2014).
7. R. Zhang and H. Hua, “Imaging quality of a retro-reflective screen in head-mounted projection displays,” J. Opt. Soc. Am. A **26**, 1240–1249 (2009).
8. J. Fergason, “Optical system for head mounted display using retroreflector and method of displaying an image,” U.S. Patent 5,621,572 (April 15, 1997).
9. R. A. Chipman, J. Shamir, H. J. Caulfield, and Q. Zhou, “Wave-front correcting properties of corner-cube arrays,” Appl. Opt. **27**, 3203–3209 (1988).
10. S. Cui, Y. Zhang, S. Y. Lim, and Y. C. Soh, “Improved accuracy of 2-D non-contact range sensors using 2-D lateral effect position sensitive detector,” Key Eng. Mater. **381**, 333–336 (2008).
11. A. L. Mieremet, R. M. A. Schleijpen, and P. N. Pouchelle, “Modeling the detection of optical sights using retro-reflection,” Proc. SPIE **6950**, 69500E (2008).
12. H. Kim and B. Lee, “Optimal design of retroreflection corner-cube sheets by geometric optics analysis,” Opt. Eng. **46**, 094002 (2007).
13. J. Nelson and D. Reed, “Retro-reflective sheeting with a corner cube surface pattern having angular corner cube circular regions,” U.S. Patent D665,584 (August 21, 2012).
14. H. Kim, S.-W. Min, and B. Lee, “Geometrical optics analysis of the structural imperfection of retroreflection corner cubes with a nonlinear conjugate gradient method,” Appl. Opt. **47**, 6453–6469 (2008).
15. M. S. Scholl, “Ray trace through a corner-cube retroreflector with complex reflection coefficients,” J. Opt. Soc. Am. A **12**, 1589–1592 (1995).
16. D. C. O’Brien, G. E. Faulkner, and D. J. Edwards, “Optical properties of a retroreflecting sheet,” Appl. Opt. **38**, 4137–4144 (1999).
17. I. Mimura, “Cube corner type retroreflection article,” U.S. Patent 8,201,953 (June 19, 2012).
18. E. Brinksmeier, R. Gläbe, and L. Schönemann, “Diamond Micro Chiseling of large-scale retroreflective arrays,” Precis. Eng. **36**, 650–657 (2012).